Quantitative analysis of strain distribution in InAs/InAs1−xSbx superlattices

Krishnamurthy Mahalingam, Elizabeth H. Steenbergen, Gail J. Brown, and Yong-Hang Zhang

Citation: Applied Physics Letters **103**, 061908 (2013); doi: 10.1063/1.4817969
View online: http://dx.doi.org/10.1063/1.4817969
View Table of Contents: http://scitation.aip.org/content/aip/journal/apl/103/6?ver=pdfcov
Published by the AIP Publishing

Quantitative analysis of strain distribution in InAs/InAs$_{1-x}$Sb$_x$ superlattices

Krishnamurthy Mahalingam,[1,a)] Elizabeth H. Steenbergen,[1] Gail J. Brown,[1] and Yong-Hang Zhang[2]
[1]*AFRL/RXAN, Materials and Manufacturing Directorate Air Force Research Laboratory, Wright-Patterson AFB, Ohio 45433-7707, USA*
[2]*School of Electrical, Computer and Energy Engineering, Arizona State University, Tempe, Arizona 85287, USA*

(Received 8 June 2013; accepted 24 July 2013; published online 8 August 2013)

Atomic resolution transmission electron microscopy is performed to examine the strain distribution in an InAs/InAs$_{1-x}$Sb$_x$ superlattice grown on a (100)-GaSb substrate. The strain profiles reveal that the thickness of tensile regions in the superlattice is significantly lower than expected, with a corresponding increase in thickness of the compressive regions. Furthermore, significant grading is observed within the tensile regions of the strain profile, indicating Sb intermixing from the InAsSb growth surface. The results signify an effective reduction in the InAs layer thickness due to the anion (As-Sb) exchange process at the InAs-on-InAsSb interface. © *2013 AIP Publishing LLC*. [http://dx.doi.org/10.1063/1.4817969]

Arsenide/antimonide based III-V semiconductor strained layer superlattices have attracted significant attention as tunable device materials for mid- to very long-wavelength infrared detection.[1–10] There are two categories of material systems: InAs/In$_x$Ga$_{1-x}$Sb superlattices, and the Ga-free InAs/InAs$_{1-x}$Sb$_x$ superlattices. While InAs/In$_x$Ga$_{1-x}$Sb superlattices have been extensively studied for over two decades,[1–5] InAs/InAs$_{1-x}$Sb$_x$ superlattices have only recently emerged as potential alternatives,[6–11] due to their superior minority carrier lifetime, which is attributed to the absence of Ga-induced Shockley-Read-Hall defects.[8–10] A critical aspect in the design and growth of these materials is balancing the superlattice strain, which needs to be performed such that, in addition to achieving high structural quality, the appropriate composition and associated strain of the constituent layers are maintained over the whole structure. Proper strain profiles across individual layers in the superlattice is particularly important for tailoring of the superlattice band structure and related properties.[4] An examination of the local strain distribution within the superlattice is then important, since it provides a direct means for investigating atomistic processes that control structural evolution during growth and for understanding how these affect key properties of the overall structure. Atomic scale strain distribution studies have been reported recently on InAs/In$_x$Ga$_{1-x}$Sb superlattices, which revealed the nature of strain localization at interfaces and surface segregation within GaSb layers.[12,13] There is, however, a lack of similar studies on InAs/InAs$_{1-x}$Sb$_x$ superlattices. The objective of the present communication is to apply recent advancements in high-resolution transmission electron microscopy (HRTEM) to examine the nature of strain distribution in InAs/InAs$_{1-x}$Sb$_x$ superlattices. The approach employed is similar to that described in recent studies,[12] wherein aberration corrected HRTEM is used in combination with advanced digital image analysis to obtain strain maps across thin layers (1–2 nm) at high spatial resolution.

[a)]E-mail: krishnamurthy.mahalingam.ctr@wpafb.af.mil. Tel.: (937) 656-5712. Fax: (937) 255-4913

The superlattice sample investigated in this study was grown on a (100)-GaSb substrate by molecular beam epitaxy, having a nominal period of 7.2 nm, with nominal thickness values of 5.8 nm for InAs and 1.5 nm for InAs$_{1-x}$Sb$_x$, and a nominal value of $x = 0.4$ for the composition. Cross-sectional samples for TEM observations along the orthogonal [011] and [0$\bar{1}$1] zone axes were prepared by conventional ion-milling, with the sample mounted on a liquid-nitrogen cooled cryo-stage. The HRTEM observations were performed using a Titan 80–300 TEM equipped with a spherical aberration (image) corrector. The constituent layers in the superlattice were examined using the negative spherical aberration (C_s) imaging (NCSI) method,[14,15] wherein the nominal value of C_s was set to $-20\,\mu$m and the images acquired at over-focus settings in the range of 6–10 nm. Under these imaging conditions, the projected atomic columns appear bright on a dark background, providing high contrast and enhanced spatial resolution of the cation and anion sublattices for precise location of the atomic columns and subsequent measurement of local lattice displacements (of the order of 10 pm).[12,14,15]

Figure 1 is an X-ray diffraction profile of the (400) reflection from the sample. The superlattice is closely lattice matched to the GaSb substrate, which is evident from the small separation in the respective peak positions. The superlattice period as measured from the superlattice satellite peaks was 7.3 nm. Figure 2(a) is a dark-field TEM image obtained using the chemically sensitive (200) reflections, wherein the InAs and InAsSb layers appear bright and dark, respectively. Measurement of the individual layer thicknesses from these images, based on the delineation of image contrast, yielded an average value of 5.5 ± 0.14 nm for the InAs layers and 1.8 ± 0.1 nm for InAsSb layers. The distinct dark contrast typically seen at interfaces in (200)—dark field images of InAs/InGaSb superlattices[16] is not observed in these structures. A profile of the intensity distribution across the layers in the superlattice, shown in Fig. 2(b), reveals consistent grading within each InAs layer, in addition to grading typically observed in the interfacial regions.

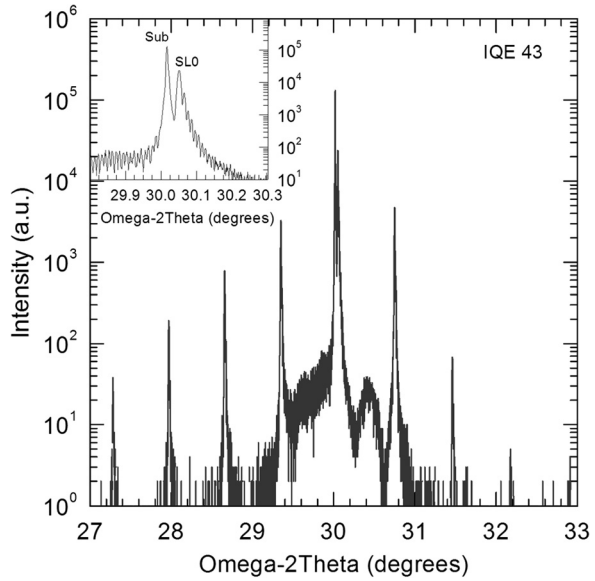

FIG. 1. (400) ω-2θ X-ray diffraction scan of the InAs/InAsSb superlattice with the inset showing the substrate peak and the superlattice zero-order peak.

Figure 3 is an HRTEM image of the superlattice structure (after applying a background subtraction filter[17] for noise removal) showing the first few layers above the substrate, wherein the bright dots in this image correspond to the projected atomic columns. To obtain the strain distribution in the superlattice, these images were further analyzed

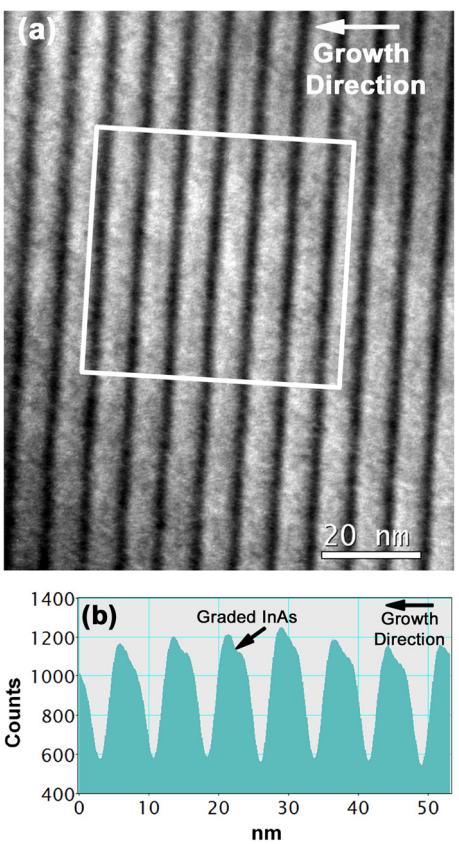

FIG. 2. (a) (200) dark-field image of the superlattice, showing the InAs (bright) and the $InAs_{1-x}Sb_x$ (dark), and (b) the intensity profile within the marked region in (a), averaged parallel to the interfaces, showing grading in the InAs layers.

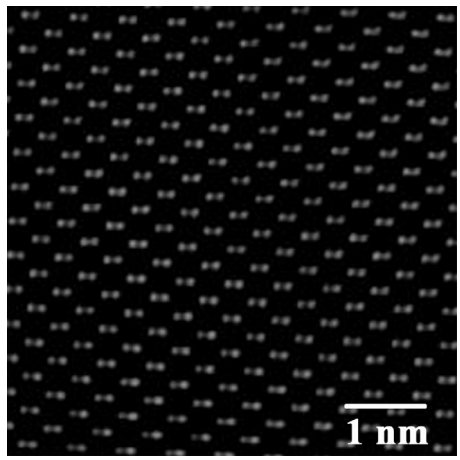

FIG. 3. A high-resolution TEM image of the superlattice where the bright dots correspond to the projected atomic columns.

by the peak-pair method,[18] using a commercial software package (HREM Research, Inc.). The procedure adopted was similar to that described in the original publication by Galindo *et al.*,[18] except that the Bragg filtering step was excluded, in order to retain all spatial frequency components contributing to the image. The analysis was performed such that the strain component ε_{xx} was parallel to the interface (along [011]) and ε_{yy} was along the growth direction ([100]). The two components were determined with respect to an averaged reference lattice in the substrate (GaSb) region.

Similar to previous studies, a detailed analysis of the maps of the two components showed that the values for ε_{xx} are negligible, thereby indicating that the interfaces are coherent.[12] Figures 4(a) and 4(b) show the map of the strain component ε_{yy} and its profile over a region including the first few periods of the superlattice adjacent to the substrate. The strain map in Fig. 4(a) clearly delineates the compressive (yellow/red) and tensile (green/blue) regions in the superlattice, corresponding to the InAsSb and InAs layers, respectively. From the strain profile shown in Fig. 4(b), the mean value of the peak strain in the InAsSb layers was measured to be 0.023, yielding a value of $x = 0.25$ for $InAs_{1-x}Sb_x$. The average superlattice period determined from peak-to-peak separation in the strain profile was 7.3 nm, in good agreement with those measured by X-ray diffraction profile and dark-field imaging. However, a measurement of the thickness of individual layers in the strain map indicated a significantly lower value of 4.66 ± 0.13 nm for the region in tensile strain and a corresponding higher value of 2.62 ± 0.05 nm for regions in compressive strain. The strain profiles thus indicate an effective reduction of over 15% in the InAs layer thickness.

To further examine the strain distribution within each layer in the superlattice, the mean strain profile was obtained from aligning by cross-correlation and averaging over the three periods in the boxed region in Fig. 4(a). The resulting profile, shown in Fig. 5, clearly reveals an asymmetric grading in the InAs layer, with a slow increase in the tensile strain at the InAs-on-InAsSb interface (right) and a relatively abrupt change from tensile to compressive strain at the InAsSb-on-InAs interface (left). The grading in strain profile

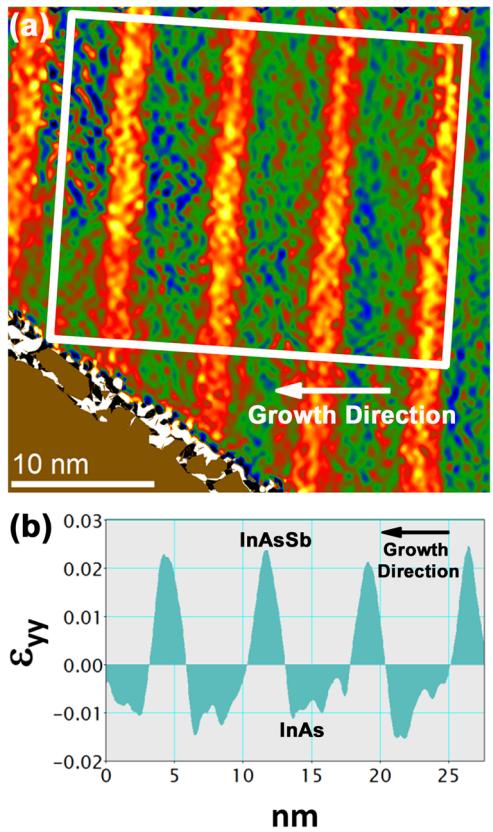

FIG. 4. (a) A strain map of the strain tensor ε_{yy}, along the growth direction, and (b) a plot of the strain profile, averaged parallel to the interface, within the marked region in (a).

observed in the vicinity of the InAs-on-InAsSb interface indicates an incorporation of Sb into InAs, most likely due to surface segregation of Sb from the InAsSb layer, induced by the As-Sb exchange reaction.[19,20] As additional support to the observed strained profile, a comparison of the intensity profile in Fig. 2(b) was performed by inverting the image in Fig. 2(a) and rescaling the pixel values to the same range as that for the strain map in Fig. 4(a). Figure 5 shows the mean intensity profile for the (inverted) (200) dark-field image, obtained from an averaging procedure similar to that for the strain profile. A direct correlation between the two profiles is evident and, given the compositional sensitivity of the zinc-blende (200) reflection,[21] clearly indicates a grading in chemical composition.

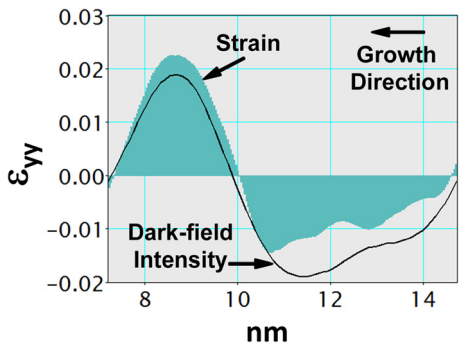

FIG. 5. Profile of the strain tensor ε_{yy} (shaded) and the (200) dark-field intensity (black line) averaged over three superlattice periods.

It is of interest to compare the above results with those reported in similar studies on InAs/$In_xGa_{1-x}Sb$ superlattices.[12,13] It is well known that strain localization at interfaces and the need to tailor interface composition plays an important role in Ga-based superlattices, due to the formation of Ga-As (tensile) and In-Sb (compressive) bonds at the interface. In the present study, however, the need for interface composition control is alleviated due to the absence of Ga in these superlattices. Indeed, a comparison of the strain profile in Fig. 4, with those reported for InAs-$In_xGa_{1-x}Sb$,[12,13] show that the strong negative spikes due to the dominant presence of Ga-As bonds (in interfaces with no composition control), are not observed herein. The present results, however, indicate that anion segregation at the InAs-on-InAsSb interface must be addressed, which should be possible by appropriate control of As/Sb and V/III flux ratios.[20]

In summary, the strain distribution across interfaces in an InAs/$InAs_{1-x}Sb_x$ superlattice was investigated by aberration corrected HRTEM. The strain profiles (ε_{yy}) revealed significant reduction in the InAs layer thickness and also compositional grading within these layers, due to the segregation of Sb from the InAsSb surface. To preserve the designed InAs layer thickness and composition, the As-Sb exchange reaction at the InAs-on-InAsSb interface must be controlled, which is important since the band gap of the superlattice and related properties are sensitive to monolayer fluctuations in its thickness.[22]

This research was sponsored by the Materials and Manufacturing Directorate, Air Force Research Laboratory, Wright-Patterson AFB, under Air Force contract FA8650-08-D-5200. The superlattice sample was grown by IQE, Inc.

[1]D. R. Rhiger, J. Electron. Mater. **40**, 1815 (2011).
[2]A. Rogalski, J. Antoszewski, and L. Faraone J. Appl. Phys. **105**, 091101 (2009).
[3]G. J. Brown, Proc. SPIE **5783**, 65 (2005).
[4]D. L. Smith and C. Mailhiot, J. Appl. Phys. **62**, 2545 (1987).
[5]G. A. Sai-Halasz, R. Tsu, and L. Esaki, Appl. Phys. Lett. **30**, 651 (1977).
[6]A. Y. Lew, E. T. Yu, and Y. H. Zhang, J. Vac. Sci. Technol. B **14**, 2940 (1996).
[7]D. Lackner, O. J. Pitts, M. Steger, A. Yang, M. L. W. Thewalt, and S. P. Watkins, Appl. Phys. Lett. **95**, 081906 (2009).
[8]E. H. Steenbergen, B. C. Connelly, G. D. Metcalfe, H. Shen, M. Wraback, D. Lubyshev, Y. Qiu, J. M. Fastenau, A. W. K. Liu, S. Elhamri, O. O. Cellek, and Y.-H. Zhang, Appl. Phys. Lett. **99**, 251110 (2011).
[9]H. S. Kim, O. O. Cellek, Z.-Y. Lin, Z.-Y. He, X.-H. Zhao, S. Liu, H. Li, and Y.-H. Zhang, Appl. Phys. Lett. **101**, 161114 (2012).
[10]B. V. Olson, E. A. Shaner, J. K. Kim, J. F. Klem, S. D. Hawkins, L. M. Murray, J. P. Prineas, M. E. Flatté, and T. F. Boggess, Appl. Phys. Lett. **101**, 092109 (2012).
[11]T. Schuler-Sandy, S. Myers, B. Klein, N. Gautam, P. Ahirwar, Z.-B. Tian, T. Rotter, G. Balakrishnan, E. Plis, and S. Krishna, Appl. Phys. Lett. **101**, 071111 (2012).
[12]K. Mahalingam, H. J. Haugan, G. J. Brown, and K. G. Eyink, Ultramicroscopy **127**, 70 (2013).
[13]H. J. Haugan, G. J. Brown, S. Elhamri, W. C. Mitchel, K. Mahalingam, M. Kim, G. T. Noe, N. E. Ogden, and J. Kono, Appl. Phys. Lett. **101**, 171105 (2012).
[14]C. L. Jia, M. Lentzen, and K. Urban, Science **299**, 870 (2003).
[15]C. L. Jia, L. Houben, A. Thust, and J. Barthel, Ultramicroscopy **110**, 500 (2010).
[16]K. Mahalingam, K. G. Eyink, G. J. Brown, D. L. Dorsey, C. F. Kisielowski, and A. Thust, J. Microsc. **230**, 372 (2008).

[17]R. Kilaas, J. Microsc. **190**, 45 (1998).
[18]P. L. Galindo, S. Kret, A. M. Sanchez, J.-Y. Laval, A. Yanez, J. Pizarro, E. Guerrero, T. Ben, and S. I. Molina, Ultramicroscopy **107**, 1186 (2007).
[19]J. Steinshnider, J. Harper, M. Weimer, C.-H. Lin, and S. S. Pei, Phys. Rev. Lett. **85**, 4562 (2000), and references therein.
[20]G. J. Sullivan, A. Ikhlassi, J. Bergman, R. E. DeWames, J. R. Waldrop, C. Grein, M. Flatté, K. Mahalingam, H. Yang, M. Zhong, and M. Weimer, J. Vac. Sci. Technol. B **23**, 1144 (2005).
[21]E. G. Bithell and W. M. Stobbs, Philos. Mag. **60**, 39 (1989).
[22]H. J. Haugan, L. Grazulis, G. J. Brown, K. Mahalingam, and D. H. Tomich, J. Cryst. Growth **261**, 471 (2004).